PROCEEDINGS OF SCIENCE

Topological susceptibility in high temperature full QCD via staggered spectral projectors

Andreas Athenodorou,[a,b] **Claudio Bonanno,**[c] **Claudio Bonati,**[a] **Giuseppe Clemente,**[d] **Francesco D'Angelo,**[a,*] **Massimo D'Elia,**[a] **Lorenzo Maio,**[a] **Guido Martinelli,**[e] **Francesco Sanfilippo**[f] **and Antonino Todaro**[g,h,i]

[a] *Università di Pisa and INFN Sezione di Pisa, Largo B. Pontecorvo 3, I-56127 Pisa, Italy*

[b] *Computation-based Science and Technology Research Center, The Cyprus Institute, 20 Kavafi Str., Nicosia 2121, Cyprus*

[c] *INFN Sezione di Firenze, Via G. Sansone 1, I-50019 Sesto Fiorentino, Firenze, Italy*

[d] *Deutsches Elektronen-Synchrotron (DESY), Platanenallee 6, 15738 Zeuthen, Germany*

[e] *Dipartimento di Fisica and INFN Sezione di Roma "La Sapienza", Piazzale Aldo Moro 5, I-00185 Rome, Italy*

[f] *INFN Sezione di Roma Tre, Via della Vasca Navale 84, I-00146 Rome, Italy*

[g] *Department of Physics, University of Cyprus, P.O. Box 20537, 1678 Nicosia, Cyprus*

[h] *Faculty of Mathematics und Natural Sciences, University of Wuppertal, Wuppertal-42119, Germany*

[i] *Dipartimento di Fisica, Università di Roma "Tor Vergata", Via della Ricerca Scientifica 1, I-00133 Rome, Italy*

E-mail: a.athenodorou@cyi.ac.cy, claudio.bonanno@fi.infn.it, claudio.bonati@unipi.it, giuseppe.clemente@desy.de, francesco.dangelo@phd.unipi.it, massimo.delia@unipi.it, lorenzo.maio@phd.unipi.it, guido.martinelli@roma1.infn.it, francesco.sanfilippo@infn.it, atodar01@ucy.ac.cy

We compute the topological susceptibility of $N_f = 2+1$ QCD at the physical point in a temperature range going from 200 to 600 MeV. We adopt a multicanonical approach to enhance topological fluctuations and a definition of the susceptibility based on the spectral projectors over the eigenmodes of the staggered Dirac operator. This method allows to reduce lattice artifacts affecting the standard gluonic definition, making the continuum limit extrapolation more reliable.

The 39th International Symposium on Lattice Field Theory,
8th-13th August, 2022,
Rheinische Friedrich-Wilhelms-Universität Bonn, Bonn, Germany

*Speaker

PoS(LATTICE2022)393

1. Introduction

Strong CP-problem is one of the most important open issues posed by the Standard Model. One of the most promising solutions is the Peccei-Quinn mechanism, that introduces a new hypothetical particle, the axion. Because of its properties, axion is also a possible candidate for Dark Matter.

The phenomenology of QCD axion is strictly related to the topological properties of QCD, and this is one of the reasons that enhanced the interest in studying them from the lattice in recent years [1–6]. For instance, the temperature-dependent axion mass is given by:

$$m_a^2(T) = \frac{\chi(T)}{f_a^2} \,, \tag{1}$$

where f_a is the axion decay constant and χ is the QCD topological susceptibility. This quantity is the second order derivative of the QCD free energy density with respect to θ in $\theta = 0$, and it is defined in the following way:

$$\chi \equiv \frac{\langle Q^2 \rangle}{V} \,, \tag{2}$$

where V is the space-time volume and Q is the topological charge, i.e., the 4D integral of the topological charge density $q(x)$,

$$q(x) = \frac{1}{32\pi^2} \varepsilon_{\mu\nu\rho\sigma} \mathrm{Tr}\{F^{\mu\nu}(x) F^{\rho\sigma}(x)\}. \tag{3}$$

There are several issues to deal with when trying to compute the topological susceptibility in the high-temperature regime. Among them, we recall the following ones:

Rare events. The topological susceptibility is expected to drop when $T \gg T_c$, this implies $\langle Q^2 \rangle = \chi(T) V \ll 1$. In other words, unless an unfeasibly large volume V is considered, configurations with non-zero value of the topological charge become very rare, and one has to collect very large statistics to precisely compute χ from the variance $\langle Q^2 \rangle$ of the topological charge distribution.

Chiral symmetry and lattice artifacts. The most frequently used fermion lattice discretizations at high-T (like the staggered one) are characterized by an explicit breaking of the chiral symmetry at finite lattice spacing. This fact leads to severe lattice artifacts in the computation of the topological susceptibility. In order to demonstrate this, the starting point is the *index theorem*, that relates the topological charge to the spectrum of the Dirac operator:

$$Q = \mathrm{Tr}\{\gamma_5\} = n_+ - n_- \,, \tag{4}$$

where n_+ (n_-) is the number of zero modes of the Dirac operator with left (right) chirality. In the continuum case, a configuration with $Q \neq 0$ has a path-integral weight proportional to

$$\det[\not{D} + m_q] = \prod_i [m_q + i\lambda_i] \,, \qquad \lambda_{min} = m_q \,. \tag{5}$$

On the lattice, chiral symmetry breaking shifts the minimum eigenvalues by $O(a^2)$ artifacts:

$$\lambda_{min} = m_q \longrightarrow m_q + i\lambda \,, \tag{6}$$

i.e., the exact zero modes of the Dirac operator become Would-Be Zero Modes (WBZM). The crucial consequence is the following: at finite lattice spacing, configurations with $Q \neq 0$ are less suppressed in the path integral than in the continuum case. This fact translates into large lattice artifacts for the topological susceptibility, and into the necessity to go to very fine lattice spacings in order to make a reliable computation.

Topological freezing. At lattice spacing of the order of ~ 0.01 fm, standard Monte Carlo algorithms remain trapped into fixed topological sectors, thus, loosing ergodicity.

In this talk, we fight against large artifacts by using a different definition of the topological susceptibility based on the spectral projectors of the staggered Dirac operator [7, 8]. We focus on the computation of the topological susceptibility at high-T and show some results of Ref. [9].

2. Lattice setup and topological charge discretizations

We simulate $N_f = 2 + 1$ QCD at the physical point moving along a Line of Constant Physics with $m_\pi \simeq 135$ MeV and $m_s/m_l \simeq 28.15$ [10–12]. We use the rooted stout staggered discretization for the fermionic sector and the tree-level Symanzik improved Wilson gauge action.

We adopt two different discretizations of the topological charge: a gluonic definition based on the straightforward discretization of $q(x)$ in terms of gauge links, and a fermionic one based on the spectral projectors on the staggered Dirac operator eigenmodes.

The gluonic definition adopted is the clover one, that has a definite parity [13, 14]:

$$Q_{\text{clov}} = \frac{-1}{2^9\pi^2}\sum_x \sum_{\mu\nu\rho\sigma=\pm 1}^{\pm 4} \varepsilon_{\mu\nu\rho\sigma}\text{Tr}\left\{\Pi^{(1\times 1)}_{\mu\nu}(x)\Pi^{(1\times 1)}_{\rho\sigma}(x)\right\} , \tag{7}$$

where $\epsilon_{\mu\nu\rho\sigma}$ is the totally antisymmetric Levi-Civita tensor with the property $\epsilon_{\mu\nu\rho\sigma} = -\epsilon_{(-\mu)\nu\rho\sigma}$. With this defintion, the topological susceptibility acquires both a multiplicative and additive renormalizations due to the presence of short range singularities:

$$\chi_{\text{gluo}} = Z_Q^2 \frac{\langle Q^2_{\text{clov}}\rangle}{V} + M_{\text{add}}. \tag{8}$$

In order to avoid to deal with these renormalization constants, smoothing procedures are usually adopted. These algorithms allow to damp UV fluctuations without changing the topological content of the gauge configurations. In other words, one has $Z_Q \simeq 1$ and $M_{\text{add}} \simeq 0$ after a certain amount of smoothing. In this work, we adopt the cooling method [15–21] and we observe that the topological susceptibility is stable after $n_{\text{cool}} \sim 100$ cooling steps. We also adopt the "α-rounding procedure" [22, 23] in order to assign an integer value to the topological charge.

Now we briefly sketch the staggered spectral projectors definition of the topological susceptibility. The starting point is the lattice version of the index theorem for staggered fermions

$$Q^{(\text{stag})}_{\text{SP, bare}} = \frac{1}{2^{d/2}}\text{Tr}\{\Gamma_5\mathbb{P}_M\} = \frac{1}{2^{d/2}}\sum_{|\lambda_k|\leq M} u_k^\dagger\Gamma_5 u_k , \qquad \not{D}_{\text{stag}}u_k = i\lambda_k u_k . \tag{9}$$

Here $\mathbb{P}_M$ is the projector on the space spanned by the eigenstates of $\not{D}_{\text{stag}}$ with eigenvalues $|\lambda| \leq M$, where M is a threshold mass. Since $\mathbb{P}_M$ cuts the UV part of the Dirac spectrum, this is basically

the reason why the spectral topological charge acquires only a multiplicative renormalization [8]:

$$Q_{\rm SP}^{(\rm stag)} = Z_{\rm SP}\, Q_{\rm SP,\,bare}^{(\rm stag)} = \sqrt{\frac{\langle {\rm Tr}\{\mathbb{P}_M\}\rangle}{\langle {\rm Tr}\{\Gamma_5 \mathbb{P}_M \Gamma_5 \mathbb{P}_M\}\rangle}}\, Q_{\rm SP,\,bare}^{(\rm stag)} \,. \tag{10}$$

At the end of the story, one computes the topological susceptibility by using the following definition

$$\chi_{\rm SP} = \frac{1}{V}\left\langle \left(Q_{\rm SP}^{(\rm stag)}\right)^2 \right\rangle \,. \tag{11}$$

Now we want to discuss the role of the cut-off mass M. First, the continuum limit of $\chi_{\rm SP}$ does not depend on the choice of the threshold mass. This is because the WBZMs become exact zero modes in the continuum limit and they are the only relevant ones from the topological point of view[1]. However, lattice artifacts do depend on this choice so one has to pay further attention. Another relevant question is how to perform the continuum limit. As explained in Ref. [7], one has to take the renormalized value of the threshold mass fixed because otherwise there is no guarantee to have $O(a^2)$ corrections.

With the staggered discretization, the renormalized threshold mass is given by $M_R = M/Z_S^{(s)}$ with $Z_S^{(s)}$ being the renormalization constant of the flavour singlet scalar current density $S_0 = \bar{\psi}\psi$. When a Line of Constant Physics is known, a direct computation of $Z_S^{(s)}$ is avoidable: indeed, the ratio between M and any quark mass is a renormalization group invariant, so one can simply fix $M/\hat{m}_q$ for each lattice spacing. In this work we normalize M to the strange quark mass $\hat{m}_s$.

The final point is how to choose M in order to make lattice artifacts as small as possible. The main idea is that, at finite lattice spacing, only WBZMs are expected to carry the relevant topological content. Being the identification of WBZMs not an easy task, one would like to include the majority of eigenmodes with an high value of the chirality, getting rid of as much noise (i.e., low chirality modes) as possible.

3. Zero temperature

In this section we report results for the zero temperature regime, where a reliable theoretical prediction for the topological susceptibility is available also from Chiral Perturbation Theory (ChPT) [24–29]. In particular, using the Next-to-Leading Order (NLO) expression of Ref. [28], one gets the estimate [1]:

$$\chi_{\rm ChPT}^{1/4} = 77.8(4)\ {\rm MeV}\,, \qquad (m_u/m_d = 1)\,. \tag{12}$$

In order to establish the optimal value for the threshold mass M/m_s, following the idea sketched in Sec. 2, we made a scatter plot of the absolute value of the chirality $r_\lambda \equiv |u_\lambda^\dagger \Gamma_5 u_\lambda|$ vs the absolute value of its eigenvalue, expressed in units of m_s, for all the computed eigenstates (Fig. 1). For $T \simeq 0$ there is not a clear separation between high and low chirality modes; however, we choose as optimal range (in the following, we will refer to it as "M-range") $M/m_s \in [0.05, 0.15]$ in order not to include in the spectral sums the tail of eigenmodes with $r_\lambda \lesssim 0.1$.

[1] This is a direct implication of the index theorem.

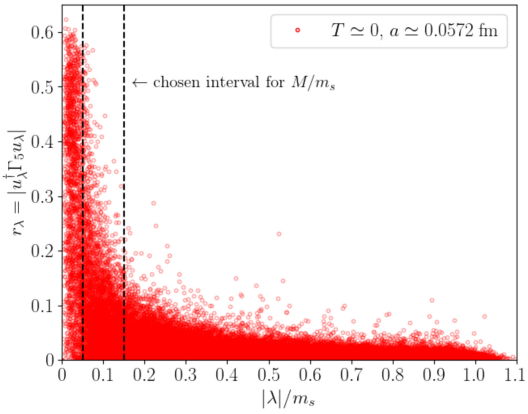

Figure 1: Scatter plot of chirality r_λ vs $|\lambda|/m_s$ for the first 200 eigenvalues of a 48^4 lattice with $a = 0.0572$ fm (finest lattice spacing available at this temperature). The two dashed vertical lines delimit the M-range. Plot taken from Ref. [9].

In order to estimate the systematics deriving from the possibility of varying the threshold mass in the M-range, the continuum limit has been performed for different values of M/m_s according to the scaling behaviour:

$$\chi_{\rm SP}^{\rm (stag)}(a, M/m_s) = \chi_{\rm SP} + c_{\rm SP}(M/m_s)a^2 + o(a^2) \ . \tag{13}$$

On the left hand side of Fig. 2, the scaling towards the continuum limit of $\chi^{1/4}$ is shown for both the gluonic and the spectral projectors definitions. One can notice that, if M/m_s is properly chosen within the M-range, then it is possible to strongly reduce lattice artifacts. On the right hand side of Fig. 2, systematic effects are shown: all the spectral determinations are compatible among them and the final spectral estimation for the topological susceptibility in the zero temperature case is:

$$\chi_{\rm SP}^{1/4}(T = 0) = 80(10) \text{ MeV} \ , \tag{14}$$

that is in agreement both with the ChPT prediction (Eq. 12) and the gluonic results obtained in Refs. [1, 9].

4. Finite temperature

The same approach followed at $T \simeq 0$ has been extended to the finite temperature case. In Ref. [9], 5 different temperatures going from 200 MeV to 600 MeV have been explored. However, in this talk, only results at $T = 430$ MeV will be shown.

When going in the high temperature regime, as mentioned in Sec. 1, $Q \neq 0$ gauge configurations become very rare. In order to fight this issue, we adopt the multicanonical approach (see Refs. [2, 30, 31] for more details). In a few words, this algorithm consists in adding to the action a bias potential in order to enhance the probability of $Q \neq 0$ configurations; finally, Monte Carlo averages with respect to the starting distribution are computed by using standard reweighting techniques.

In the following, we present results about the computation of $\chi_{\rm SP}^{1/4}$ at $T \simeq 430$ MeV. In Fig. 3 (left), we show the scatter plot of r_λ and $|\lambda|/m_s$. A separation between high and low chirality modes

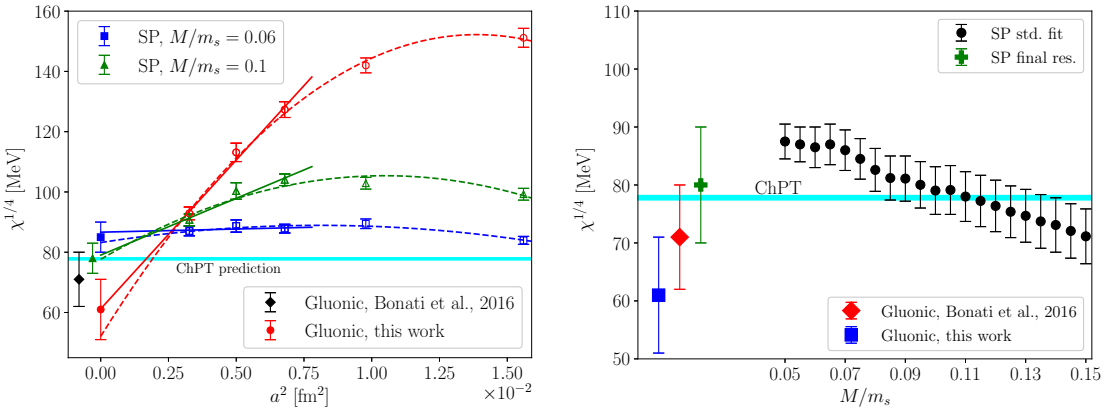

Figure 2: Left: Continuum scaling of $\chi^{1/4}$. The horizontal band stands for the NLO ChPT prediction in Eq. (12). The diamond full point stands for the gluonic determination reported in Ref. [1]. Right: evaluation of the systematics related to the choice of M/m_s within the M-range. The cross point represents our final SP determination of $\chi^{1/4}$. The diamond full point represents the gluonic determination obtained in Ref. [1]. Plots taken from Ref. [9].

is clearly visible, and we choose as M-range $M/m_s \in [0.3, 5]$ in order not to include in spectral sums the cluster of low chirality modes. In Fig. 3 (right) the continuum scaling of $\chi^{1/4}$ is shown for both the gluonic and the SP definitions. The same conclusions of the $T \simeq 0$ case still holds, i.e., the SP definition allows to reduce lattice artifacts if M/m_s is properly choosen.

In Fig. 4 (left), $\chi_{\rm SP}$ for several values of M/m_s is plotted. All SP determinations are compatible among them and the final SP estimation is:

$$\chi^{1/4}_{\rm SP}(T \simeq 430\ \text{MeV}) = 15(5)\ \text{MeV}\ , \tag{15}$$

where the error takes into account all the systematic and statistical uncertainties. This value is compatible with the gluonic estimation ($\chi^{1/4}_{\rm gluo}(T \simeq 430\ \text{MeV}) = 14(5)$ MeV). In Fig. 4 (right), the quantity $c_{\rm SP}/c_{\rm gluo}$ is plotted for different values of M/m_s within the M-range. This is just the value of the coefficent of order a^2 in Eq. (13) of the SP case, normalized to its gluonic counterpart. It is worth noticing that there are values of M/m_s for which this ratio is compatible with zero, and that this ratio increases when M/m_s grows, pointing out that noise (i.e., non-chiral modes) has been introduced into the spectral sums.

4.1 Power law behaviour of the topological susceptibility

According to the Dilute Instanton Gas Approximation (DIGA), at $T \gg T_c$ the topological susceptibility is expected to decay according to $\chi^{1/4} \propto T^{-b}$ with $b_{\rm DIGA} \sim 2$. We compared our results with the DIGA prediction (Fig. 5). Fitting all available points, we obtain

$$b_{\rm SP} = 1.82(43), \qquad b_{\rm gluo} = 1.67(51)\ .$$

They are compatible both with DIGA prediction and with the value $b_{\rm BW} = 1.945(23)$ obtained by fitting all values in Ref. [4] for $T \gtrsim 170$ MeV. However, we observe a 2-3 standard deviation tension with results of Ref. [4, 5] in the range 300 MeV $\lesssim T \lesssim$ 400 MeV.

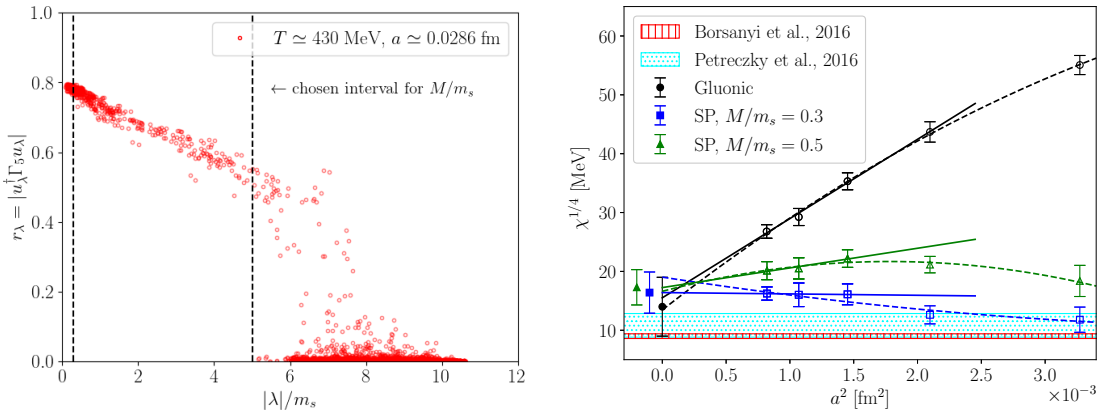

Figure 3: Left: scatter plot of chirality r_λ vs $|\lambda|/m_s$ for the first 200 eigenvalues of a run with $a = 0.0286$ fm at $T = 430$ MeV. The two dashed vertical lines delimit the M-range. Right: Continuum scaling of $\chi^{1/4}$ for both the gluonic (circled points) and the spectral projectors (triangle and square-shaped points). Only two values of M/m_s in the M-range are showed. Vertically-hatched and dotted-hatched bands stand for the estimations obtained in Refs. [4, 5]. The latter has been scaled according to $\chi^{1/4} \sim m_\pi$. Plots taken from Ref. [9].

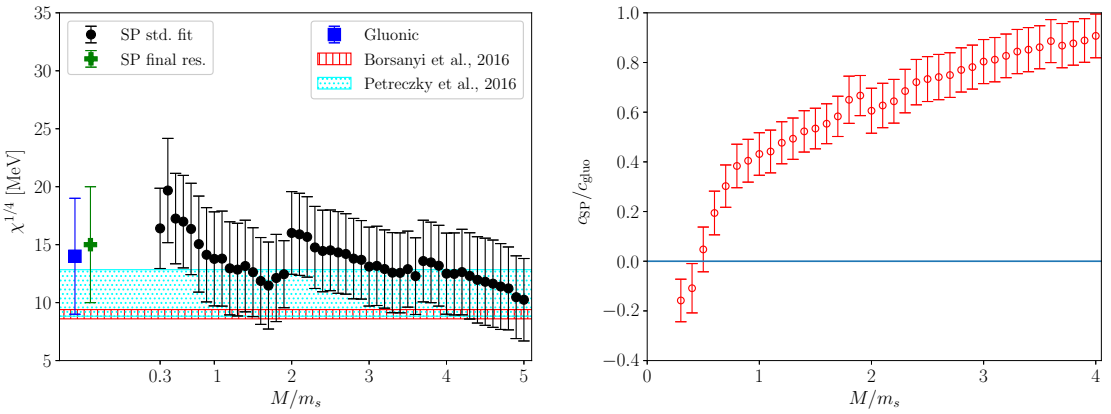

Figure 4: Left: Systematics related to M/m_s within the M-range for $T = 430$ MeV. The cross point stands for the final SP determination while the squared point for the gluonic one. Vertically-hatched and dotted-hatched bands have the same meaning of Fig. 3. Right: $c_{\text{gluo}}/c_{\text{SP}}$ for different values of M/m_s within the M-range. Plots taken from Ref. [9].

5. Conclusions

We computed the topological susceptibility both in the zero and the finite temperature regime by using a definition based on staggered spectral projectors. The zero temperature case is a useful test for the solidity of our procedure, and we found our spectral result to be in agreement with the well-established ChPT prediction.

For this reason, we extended our analysis to the high-temperature regime. In this case, unlike at zero temperature, we also adopted the multicanonical algorithm in order to compute the topological susceptibility more efficiently. We found in all cases that the SP definition allows to reduce lattice

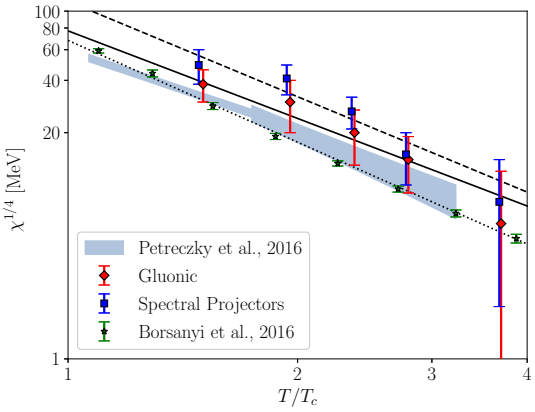

Figure 5: $\chi^{1/4}$ as a function of T/T_c in double-log scale. Both gluonic and SP data are plotted. Gluonic points are slightly shifted to improve readability. The grey area refers to the results obtained in Ref. [5] properly rescaled according to $\chi^{1/4} \sim m_\pi$. Starred points are those of Ref. [4] without isospin breaking factor. Plot taken from Ref. [9].

artifacts with respect to the gluonic definition. In particular, the choice of the free parameter M/m_s provides a better control on the systematics related to the continuum extrapolation.

We finally compared our $T > T_c$ results with the DIGA prediction and we found very good agreement. However, in the range 300 MeV $\lesssim T \lesssim$ 400 MeV, we observed a 2-3 standard deviation tension with results of Refs. [4, 5]. For this reason, in order to better clarify this apparent discrepancy, in the future we could refine our analysis in this temperature range by adding a finer lattice spacing. Furthermore, it would be interesting also to explore the region around $T \sim 1$ GeV, that is relevant for axion cosmology. However, these tasks require very fine lattice spacings (of the order of $a \sim 0.01$ fm) and topological freezing has to be properly treated. A promising solution to this issue is the *parallel tempering on boundary conditions* [32–35].

References

[1] C. Bonati, M. D'Elia, M. Mariti, G. Martinelli, M. Mesiti, F. Negro et al., *Axion phenomenology and θ-dependence from $N_f = 2 + 1$ lattice QCD*, *JHEP* **03** (2016) 155 [1512.06746].

[2] C. Bonati, M. D'Elia, G. Martinelli, F. Negro, F. Sanfilippo and A. Todaro, *Topology in full QCD at high temperature: a multicanonical approach*, *JHEP* **11** (2018) 170 [1807.07954].

[3] M. P. Lombardo and A. Trunin, *Topology and axions in QCD*, *Int. J. Mod. Phys. A* **35** (2020) 2030010 [2005.06547].

[4] S. Borsanyi et al., *Calculation of the axion mass based on high-temperature lattice quantum chromodynamics*, *Nature* **539** (2016) 69 [1606.07494].

[5] P. Petreczky, H.-P. Schadler and S. Sharma, *The topological susceptibility in finite temperature QCD and axion cosmology*, *Phys. Lett. B* **762** (2016) 498 [1606.03145].

[6] A. Y. Kotov, A. Trunin and M. P. Lombardo, *QCD topology and axion's properties from Wilson twisted mass lattice simulations*, *PoS* **LATTICE2021** (2022) 032 [2111.15421].

[7] L. Giusti and M. Lüscher, *Chiral symmetry breaking and the Banks-Casher relation in lattice QCD with Wilson quarks*, *JHEP* **03** (2009) 013 [0812.3638].

[8] C. Bonanno, G. Clemente, M. D'Elia and F. Sanfilippo, *Topology via spectral projectors with staggered fermions*, *JHEP* **10** (2019) 187 [1908.11832].

[9] A. Athenodorou, C. Bonanno, C. Bonati, G. Clemente, F. D'Angelo, M. D'Elia et al., *Topological susceptibility of $N_f = 2 + 1$ QCD from staggered fermions spectral projectors at high temperatures*, *JHEP* **10** (2022) 197 [2208.08921].

[10] Y. Aoki, S. Borsanyi, S. Durr, Z. Fodor, S. D. Katz, S. Krieg et al., *The QCD transition temperature: results with physical masses in the continuum limit II.*, *JHEP* **06** (2009) 088 [0903.4155].

[11] S. Borsanyi, G. Endrodi, Z. Fodor, A. Jakovac, S. D. Katz, S. Krieg et al., *The QCD equation of state with dynamical quarks*, *JHEP* **11** (2010) 077 [1007.2580].

[12] S. Borsanyi, Z. Fodor, C. Hoelbling, S. D. Katz, S. Krieg and K. K. Szabo, *Full result for the QCD equation of state with 2+1 flavors*, *Phys. Lett. B* **730** (2014) 99 [1309.5258].

[13] P. Di Vecchia, K. Fabricius, G. C. Rossi and G. Veneziano, *Preliminary Evidence for $U(1)_A$ Breaking in QCD from Lattice Calculations*, *Nucl. Phys. B* **192** (1981) 392.

[14] P. Di Vecchia, K. Fabricius, G. Rossi and G. Veneziano, *Numerical Checks of the Lattice Definition Independence of Topological Charge Fluctuations*, *Phys. Lett. B* **108** (1982) 323.

[15] B. Berg, *Dislocations and Topological Background in the Lattice $O(3)$ σ Model*, *Phys. Lett. B* **104** (1981) 475.

[16] Y. Iwasaki and T. Yoshie, *Instantons and Topological Charge in Lattice Gauge Theory*, *Phys. Lett. B* **131** (1983) 159.

[17] S. Itoh, Y. Iwasaki and T. Yoshie, *Stability of Instantons on the Lattice and the Renormalized Trajectory*, *Phys. Lett. B* **147** (1984) 141.

[18] M. Teper, *Instantons in the Quantized $SU(2)$ Vacuum: A Lattice Monte Carlo Investigation*, *Phys. Lett. B* **162** (1985) 357.

[19] E.-M. Ilgenfritz, M. Laursen, G. Schierholz, M. Müller-Preussker and H. Schiller, *First Evidence for the Existence of Instantons in the Quantized $SU(2)$ Lattice Vacuum*, *Nucl. Phys. B* **268** (1986) 693.

[20] M. Campostrini, A. Di Giacomo, H. Panagopoulos and E. Vicari, *Topological Charge, Renormalization and Cooling on the Lattice*, *Nucl. Phys. B* **329** (1990) 683.

[21] B. Alles, L. Cosmai, M. D'Elia and A. Papa, *Topology in 2D CP^{N-1} models on the lattice: A Critical comparison of different cooling techniques*, *Phys. Rev. D* **62** (2000) 094507 [hep-lat/0001027].

[22] L. Del Debbio, H. Panagopoulos and E. Vicari, *theta dependence of $SU(N)$ gauge theories*, *JHEP* **08** (2002) 044 [hep-th/0204125].

[23] C. Bonati, M. D'Elia and A. Scapellato, *θ dependence in $SU(3)$ Yang-Mills theory from analytic continuation*, *Phys. Rev. D* **93** (2016) 025028 [1512.01544].

[24] P. Di Vecchia and G. Veneziano, *Chiral Dynamics in the Large n Limit*, *Nucl. Phys. B* **171** (1980) 253.

[25] H. Leutwyler and A. V. Smilga, *Spectrum of Dirac operator and role of winding number in QCD*, *Phys. Rev. D* **46** (1992) 5607.

[26] TWQCD collaboration, Y.-Y. Mao and T.-W. Chiu, *Topological Susceptibility to the One-Loop Order in Chiral Perturbation Theory*, *Phys. Rev. D* **80** (2009) 034502 [0903.2146].

[27] F.-K. Guo and U.-G. Meißner, *Cumulants of the QCD topological charge distribution*, *Phys. Lett. B* **749** (2015) 278 [1506.05487].

[28] G. Grilli di Cortona, E. Hardy, J. Pardo Vega and G. Villadoro, *The QCD axion, precisely*, *JHEP* **01** (2016) 034 [1511.02867].

[29] F. Luciano and E. Meggiolaro, *Study of the theta dependence of the vacuum energy density in chiral effective Lagrangian models at zero temperature*, *Phys. Rev. D* **98** (2018) 074001 [1806.00835].

[30] P. T. Jahn, G. D. Moore and D. Robaina, *$\chi_{top}(T \gg T_c)$ in pure-glue QCD through reweighting*, *Phys. Rev. D* **98** (2018) 054512 [1806.01162].

[31] C. Bonanno, M. D'Elia and F. Margari, *The topological susceptibility of the 2d CP^1 ($\mathrm{O}(3)$ non-linear σ) model: to ∞ or not to ∞?*, 2208.00185.

[32] M. Hasenbusch, *Fighting topological freezing in the two-dimensional CP^{N-1} model*, *Phys. Rev. D* **96** (2017) 054504 [1706.04443].

[33] M. Berni, C. Bonanno and M. D'Elia, *Large-N expansion and θ-dependence of 2d CP^{N-1} models beyond the leading order*, *Phys. Rev. D* **100** (2019) 114509 [1911.03384].

[34] C. Bonanno, C. Bonati and M. D'Elia, *Large-N $SU(N)$ Yang-Mills theories with milder topological freezing*, *JHEP* **03** (2021) 111 [2012.14000].

[35] C. Bonanno, M. D'Elia, B. Lucini and D. Vadacchino, *Towards glueball masses of large-N $\mathrm{SU}(N)$ pure-gauge theories without topological freezing*, *Phys. Lett. B* **833** (2022) 137281 [2205.06190].